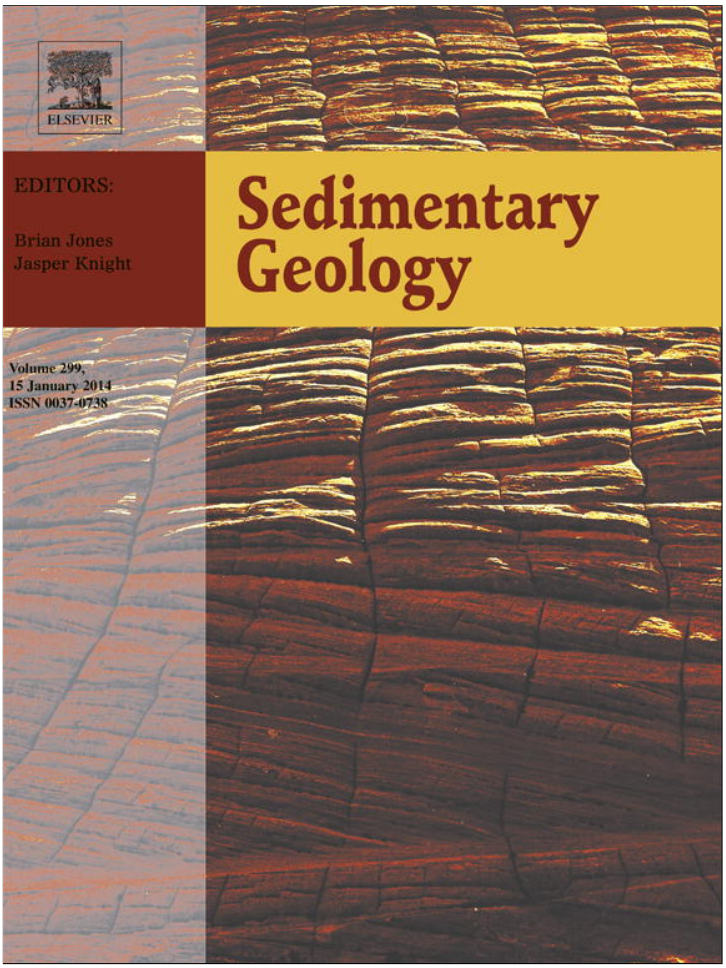

Sedimentary Geology 299 (2014) 30–41

Contents lists available at ScienceDirect

Sedimentary Geology

journal homepage: www.elsevier.com/locate/sedgeo

Provenance and burial history of cement in sandstones of the Northbrook Formation (Carboniferous), western Newfoundland, Canada: A geochemical investigation

Nigel J.F. Blamey [a,b,c,*], Karem Azmy [a,**], Uwe Brand [c]

[a] Department of Earth Sciences, Memorial University of Newfoundland, St. John's, Newfoundland A1B 3X5, Canada
[b] Department of Earth and Environmental Science, New Mexico Institute of Mining and Technology, Socorro, NM 87801, USA
[c] Department of Earth Sciences, Brock University, St. Catharines, Ontario L2S 3A1, Canada

ARTICLE INFO

Article history:
Received 11 July 2013
Received in revised form 7 October 2013
Accepted 8 October 2013
Available online 17 October 2013

Editor: B. Jones

Keywords:
Diagenesis
Cements
Fluid inclusions
Sandstones
Geochemistry
Newfoundland

ABSTRACT

The Carboniferous North Brook Formation (western Newfoundland, Canada) consisting of fluvial/lacustrine arkosic litharenites has undergone two cementation cycles. The first cycle comprises chlorite followed by minor quartz and calcite. Mono-phase aqueous fluid inclusions hosted in first-cycle calcite reflect precipitation in a near-surface meteoric diagenetic environment. Chlorite linings and cements generally inhibit precipitation of quartz overgrowths, thus maintaining open pore space until a subsequent cycle when temperatures are within the oil window. The second cycle comprises chlorite followed by calcite which hosts two-phase fluid inclusions with homogenization temperatures ranging from 91.7 to 120.7 °C and salinity from 6.3 to 8.4 eq. wt.% NaCl. These results suggest conditions in-line with a deep burial environment, and calculated fluid inclusion isochors stipulate a trapping temperature of around 132 °C and pressure of 500 bar (5 km hydrostatic pressure) for these cements. Quantitative fluid inclusion gas analysis further confirms that fluids were sourced from evolved meteoric fluids with fluctuating CO_2:CH_4:N_2 ratios. Manganese analysis confirms an oxidizing environment for the first-cycle calcite cement but a reducing one for the infilling second-cycle cement. Both cements have similar REE signatures, are slightly LREE-depleted, and during migration the fluids were influenced by the sedimentary host rock. Although there is a prominent negative Ce anomaly, there is no Eu anomaly in the cements. The $\delta^{13}C$ and $\delta^{18}O$ values are mostly in the negative in the calcite cement hosted in the coarse-grained clastics, which were influenced by migrating brines and/or hydrocarbons.

In the diagenetic history of this sedimentary basin, the first cementation event is characterized by chlorite, quartz and calcite emplaced under shallow, oxidizing meteoric water conditions and appropriate temperatures. A diagenetic hiatus ensued until the units were more deeply buried. At this stage, a second generation of cement characterized by minor chlorite and major calcite, infilled vugs and voids under higher temperatures equivalent to the upper limit of the oil window and 5 km burial depth. The lack of porosity precludes the North Brook Formation from being a petroleum reservoir although limited petroleum may have been sourced during the geologic history.

1. Introduction

Diagenetic cements play a significant role in petroleum reservoir systems by reducing pore space. Associated chlorite cements and pore infilling have been recognized in many sedimentary basins, in addition to replacement of clays by chlorite (Larsen and Friss, 1991; Tang et al., 1997; Billault et al., 2003; Kim et al., 2007; Wolela and Gierlowski-Kordesch, 2007; Mansurbeg et al., 2008; Berger et al., 2009; Peng et al., 2009; Friis et al., 2010; Karim et al., 2010; Friss et al., in press). These sedimentary environments share common characteristics that include: shallow environments, low temperature, fluvial/lacustrine settings, and a source of Fe to stabilize the mineral phases. Investigation of calcite cements and the associated chlorite linings and cements is therefore important to understanding the potential porosity retention and offers insights into petroleum migration or reservoir potential.

The Carboniferous sandstones of the North Brook Formation, Deer Lake Group have become progressively a potential target for petroleum exploration in Western Newfoundland (Langdon and Hall, 1994; Cooper et al., 2001). However, little has been forthcoming about the origin of cements and their diagenetic environments, a significant factor in better understanding the controls on porosity distribution.

* Correspondence to: N.J.F. Blamey, Department of Earth Sciences, Brock University, St. Catharines, Ontario L2S 3A1, Canada. Tel.: +1 709 864 8142; fax: +1 709 864 7437.
** Corresponding author. Tel.: +1 709 864 8142; fax: +1 709 864 7437.
E-mail addresses: nblamey@ees.nmt.edu (N.J.F. Blamey), kazmy@mun.ca (K. Azmy).

0037-0738/$ – see front matter © 2013 Elsevier B.V. All rights reserved.
http://dx.doi.org/10.1016/j.sedgeo.2013.10.005

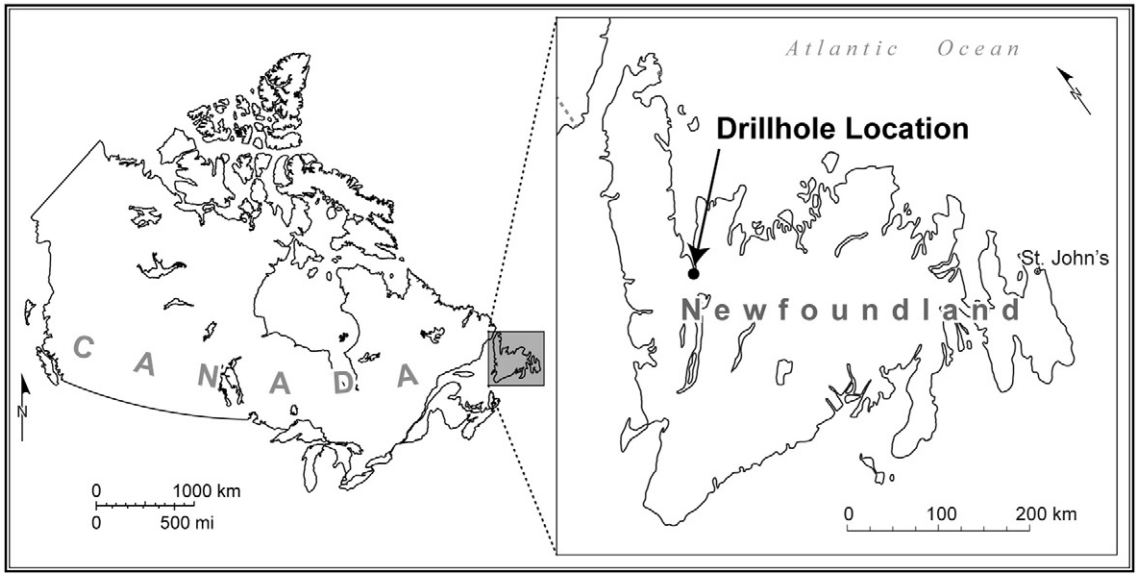

Fig. 1. Locality map of Newfoundland and Labrador. The solid circle shows the location of the Western Adventure #1 drillhole at coordinates W57° 14′ 10″ and latitude N49° 15′ 46″.

In addition to petrographic features, cements retain characteristic encrypted chemical signatures that offer vital clues to the diagenetic history.

The main objectives of the current study are:

(1) To investigate the origin and environment of formation of diagenetic cements in the North Brook Formation, particularly calcite,
(2) To better understand the paragenetic sequence of the multiple cementation events and their influence on porosity distribution, and
(3) To shed light on whether fluid temperatures reached the oil window during cementation and thus provide clues as to whether the North Brook Formation could have been a petroleum source, pathway or reservoir.

2. Geological setting

The North Brook Formation sandstones are braided stream deposits (Awadallah, 1988) and their lithostratigraphy has been described in a few earlier studies by (Awadallah, 1988; Hyde, 1989; Williams and Burden, 1992; Knight and Boyce, 2002). However, no detailed mineralogical/petrographic studies describing cements of the North Brook Formation have been yet documented. The Deer Lake Basin lies along the northeasterly-trending strike-slip Cabot Fault Zone in Western Newfoundland (Fig. 1). Lateral movement between fault branches varies but an overall displacement of up to 120 km is suggested (Hyde, 1989; Knight and Boyce, 2002). Despite the strike-slip movement affecting the Anguille Group, there is no evidence suggesting cessation of movement prior to the deposition of North Brook sediments (Knight and Boyce, 2002).

Sediments of the Anguille Group represent two stages, the first being deposits within a pull-apart basin and subsequent infill of a deep basin that formed under semiarid climatic conditions (Knight, 1983). The Anguille Group includes a Devonian to Early Carboniferous sequence of lacustrine sediments, which form the lowermost part of the Deer Lake Basin (Fig. 2). It consists of fluvial and alluvial fan sediments of estimated 3000 m thickness (Hyde, 1983, 1984, 1989).

The Deer Lake Group consists of the North Brook Formation, the Rocky Brook Formation, and either the Little Pond (western basin) or the Humber Falls Formation (eastern basin) in ascending order, unconformably overlying the Anguille Group (Hyde, 1983, 1984, 1989) (Fig. 2). The group formed in lacustrine deltaic, fluvial, and alluvial fan environments (Hyde, 1989).

Tectonic deformation in the Deer Lake area occurred during the Appalachian–Caledonian orogeny, resulting from opening and closure of the proto-Atlantic Ocean Hyde et al. (1988), Hyde (1989), Irving and Strong (1989), Knight and Boyce (2002), Knight (2003), and Burden et al. (2005). Prior to tearing apart of the present Atlantic Ocean, the continental collision zone was represented by the continuous Appalachian–Caledonian fold belt with transtensional and

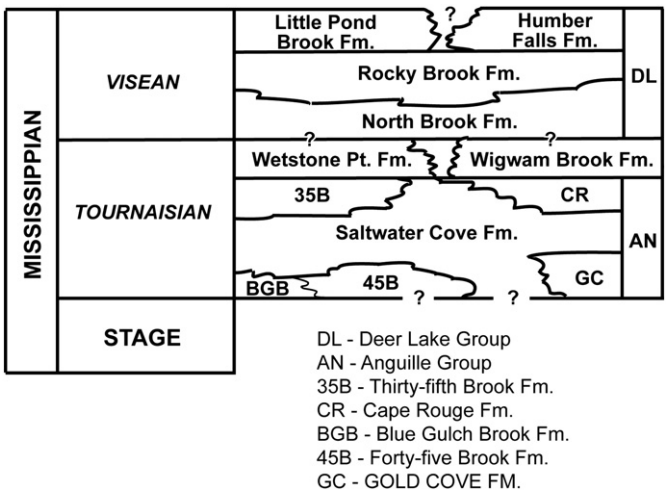

Fig. 2. Stratigraphic framework of the Deer Lake basin area, western Newfoundland (after Hyde, 1983).

Table 1
Percentages of major minerals determined by MLA using the SEM facility at CREAIT, Memorial University of Newfoundland. MLA discriminates between minerals but does not recognize the petrographic affiliation hence optical petrography is used to discriminate quartz from lithic grains. Chlorite and chloritoids are combined and grouped as chlorite. All other minerals are combined as "others".

Sample	Albite	Microcline	Quartz	Calcite	Chlorite	Others
1-799	13.9	12.1	35.4	0.3	27.3	11.0
1-855	26.1	15.9	37.4	10.2	4.8	5.6
1-964	19.2	16.0	34.8	12.3	11.2	6.5

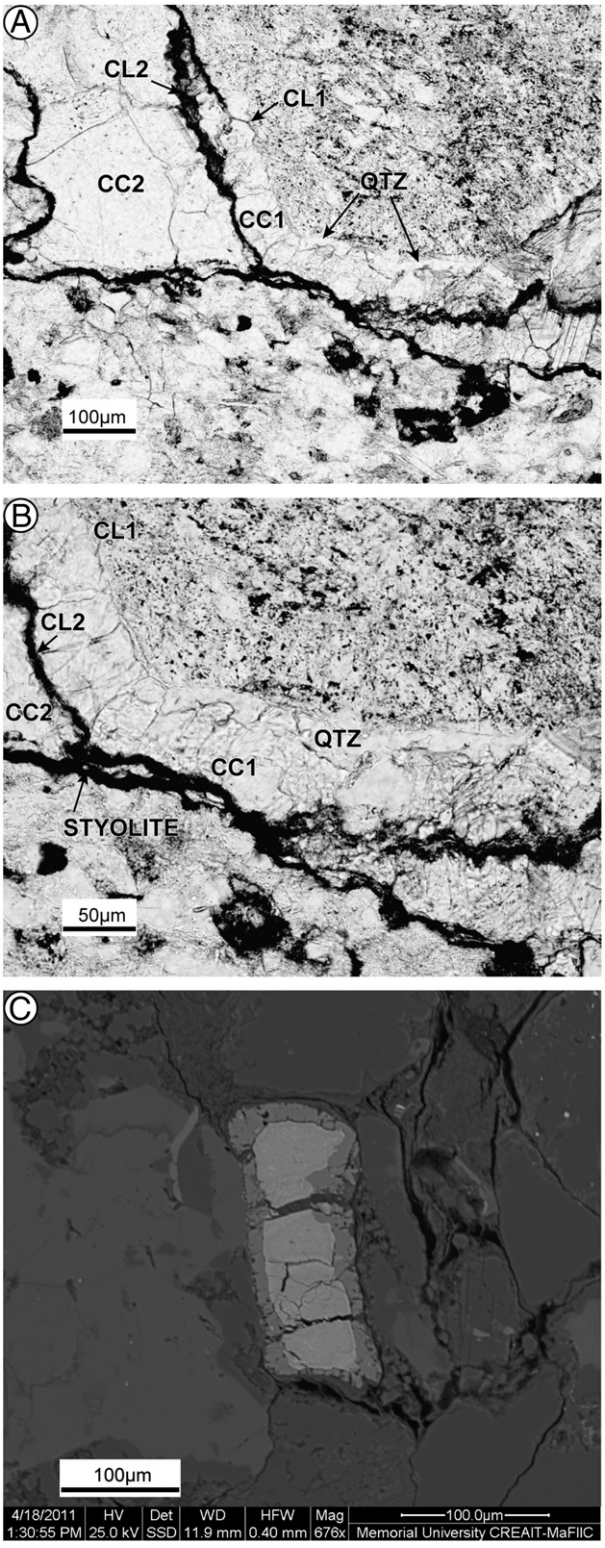

Fig. 3. (A&B) Photomicrograph showing the complete cement paragenesis (Sample 1-800, plain light). Stage 1 consists of chlorite (CL1) with a greenish stain and followed by quartz (QTZ) growth and finally fine-grained calcite (CC1). Stage 2 has a thicker chlorite cement (CL2) and is followed by infilling of coarse-grained calcite (CC2) that commonly engulfs sand grains. In all cases where quartz cement has nucleated, the substrate mineral is feldspar. The lower portion of the photomicrograph shows a lithic grain and in this case no quartz cement has developed, hence chlorite cements (CL1 and CL2) are directly precipitated onto the lithic grain. Development of styolites is evident and the organic material on the styolite surface does not respond to UV light and is inferred to be a bitumen residue. (C) Backscatter image using SEM of an ilmenite grain that has become armored by sphene, suggesting a diagenetic process. The replacement of ilmenite by sphene requires addition of silica and calcium, both of which were available during the first cementation cycle.

later transpressional strike-slip faults. The Carboniferous Deer Lake Group was controlled by the Cabot Fault zone, a zone of strike-slip faults that produced "flower" structures during transpressional regimes (Hyde et al., 1988). The Anguille Group formed during active faulting, whereas the Deer Lake Group after cessation of the movement.

3. Methods

Samples were collected from the North Brook Formation of the Western Adventure #1 drill core (Fig. 1), which is stored at the Tors Cove core facility, and described by Awadallah (1988). Our sample identification protocol corresponds to the drillhole number followed by the depth in meters. A total of 45 thin sections for petrographic examinations, fluid inclusion wafers and mounts for other analytical analyses were taken parallel to the core axis. Care was taken to minimize breakage and thereby preserve cements, texture and fabric. Samples for thin section petrography were impregnated with blue resin to highlight their porosity.

Petrographic examination was performed on a Nikon Eclipse E600POL microscope with 2×, 4×, 10×, 20×, and 40× lenses to identify textures and mineral compositions as well as characterize the relationship between different cements. Photomicrographs were taken using an attached Nikon DXM1200F digital camera. Fluid inclusion microscopy was performed using a Nikon microscope with 10× and 20× lenses, as well as a long-focusing 50× lenses.

Quantitative mineral liberation analysis (MLA) was performed using the scanning electron microscope (SEM) facility at CREAIT, Memorial University of Newfoundland. The electron beam has an acceleration energy of 25 kV which is sufficient to generate x-rays from the sample. The technique relies on backscattered electrons of polished sections to define mineral grain boundaries, and then analyzes x-ray emission with an energy dispersive detector to assign mineral compositions. This results in a mineral map of the sample and the precise evaluation of mineral content (Table 1).

Fluid inclusion microthermometry was conducted using a Linkham THMSG 600 stage with 0.1 °C precision at 0 °C. Calibration was done on a daily basis using a CO_2 standard for −56.6 °C whereas a water standard was used for ice melting at 0.0 °C and the critical point at 374.1 °C.

Cathodoluminescence was performed on polished and uncovered wafers at the University of Windsor, Ontario, using a Technosyn cold cathodoluminoscope operated at about 12 kV accelerating voltage and about 0.7 mA gun current intensity.

Gas analysis of inclusions was done in vacuum using the CFS (crush-fast scan) method described in Parry and Blamey (2010); Blamey (2012); and Azmy and Blamey (2013). Samples were first cleaned with NaOH or KOH to remove surface organics, rinsed several times with deionized water and were then dried at room temperature overnight. Approximately 150 mg of sample was crushed incrementally under a vacuum of ~10^{-8} Torr producing 6 to 10 successive bursts. The act of incremental crushing is thought to liberate calcite-hosted gases owing to the soft nature of calcite whereas that of progressive crushing contributes from quartz-hosted inclusions. To recognize gas signatures from quartz-hosted inclusions, samples were subjected to acid to dissolve the calcite cements which enables to characterize gas contributions from solely detrital grains. Data acquisition was performed by means of two Pfeiffer Prisma quadrupole mass spectrometers operating in fast-scan, peak-hopping mode. Routinely the system analyses for the following: H_2, He, CH_4, H_2O, N_2, O_2, H_2S, Ar, CO_2, C_2H_4, C_2H_6, SO_2, C_3H_6, C_3H_8, C_4H_8, C_4H_{10}, and benzene. The instrument was calibrated using commercial gas mixtures, synthetic inclusions filled with gas mixtures, and three in-house fluid inclusion gas standards as described by Norman and Blamey (2001). The amount of each species is calculated by proprietary software to provide a quantitative analysis. H_2 can be reliably detected above 50 ppm. Based on the formulae presented by Blamey et al. (2012) and applied to

aqueous-dominated fluid inclusions, the 3σ detection limit for most inorganic gas species is between 0.15 and 0.2 ppm.

Analysis of C and O stable isotopes was performed by conventional CO_2 liberation from samples. Several samples were microsampled with a low-speed microdrill to recover calcite cements. The microdrill bit was cleaned between samples to prevent contamination and a fresh paper was used for each sample that allowed collection and transfer to vials. For C- and O-isotopic analysis, typically 2 mg (in the case of some samples as much as 15 mg) of powder sample was reacted in inert atmosphere with ultrapure concentrated (100%) orthophosphoric acid at 70 °C in a Thermo-Finnigan Gasbench II. The CO_2 produced from the reaction was automatically flushed in a stream of helium through a chromatographic column and delivered to the source of a Thermo-Finnigan DELTA V plus isotope ratio mass spectrometer. In the mass spectrometer the gas was ionized and measured for isotope ratios. Uncertainties of better than 0.1‰ (2σ) for the analyses were determined by repeated measurements of NBS-19 ($\delta^{18}O = -2.20‰$ and $\delta^{13}C = +1.95‰$ vs. VPDB), CBM ($\delta^{18}O = -8.58‰$ and $\delta^{13}C = +0.75‰$ vs. VPDB), and MUN-CO-1 ($\delta^{18}O = -13.40‰$ and $\delta^{13}C = -21.02‰$ vs. VPDB) as well as internal standards during each run of samples.

The Secondary Ion Mass Spectrometer (SIMS) at CREAIT, Memorial University of Newfoundland, was used to analyze selected minor, trace and rare earth elements (REE). The technique is described by Denniston et al. (1997) whereby $^{16}O^-$ ions are accelerated by a nominal 10 kV and focused onto a gold-coated polished surface. The collision of the $^{16}O^-$ ions with the target generates secondary ions from the target which are then detected by quadrupole mass spectrometers. In-house standards with known minor, trace and REE composition are analyzed daily prior to analysis of the samples and stable isotopes are analyzed separately owing to $^{16}O^-$ ions being used for elemental analysis versus $^{133}Cs^+$ ions used for $\delta^{18}O$ isotope analysis. The ion beam is capable of conducting a 10 μm point analysis.

4. Results

4.1. Petrography of cements

Three cement types generally occur throughout the North Brook sandstones, including calcite (early and late), chlorite, and quartz. An early phase of near-micritic calcite (4–100 μm) precedes the late coarse calcite (50 μm–1 mm), which occludes the majority of pores. Diagenetic chlorite occurs in all samples as staining or as 1 to 5 μm-thick cement, which is followed by calcite infilling (Fig. 3A&B). Several grain coatings could be examined in more detail due to the fortuitous orientation of quartz grains viewed down the c-axis and in these cases the extinction angle of chlorite is perpendicular to the surface of the quartz grain. Perpendicular growth in chlorite cements has been also reported by Peng et al. (2009) from the Sichuan Basin in China and from reservoir sandstones by Billault et al. (2003).

Quartz cements are rare, but in a few cases (e.g., samples 1-800 and 1-855) feldspar-hosted fractures are infilled by quartz and fine-grained calcite. Euhedral quartz crystals (5–10 μm) might sometimes exhibit growth into open space from the surface of feldspar with subsequent infilling of the open space by calcite. Confirmation of quartz rather than feldspar is based on cathodoluminescence. Quartz infilling fractures within feldspar are observed in samples 1-749 and 1-800, and is a similar feature to fracture induced by compaction followed by filling (Friis et al., 2010). Microcrystalline quartz also occurs in sandstones of the North Sea (McBride, 1989; Ramm and Forsberg, 1991; Vagle et al., 1994; Aase et al., 1996; Aase and Walderhaug, 2005; Stokkendal et al., 2009; Weibel et al., 2010) and a similar phenomenon with the addition of other phases has been observed in other basins (e.g., Wang et al., 2008; Karim et al., 2010). In all cases, calcite that infills all pore space postdates chlorite and quartz cements.

The petrographic examination and crosscut relationships between mineral grains allows the reconstruction of the paragenetic sequence of cement formation (Fig. 4). A thin green staining of chlorite developed on the surface of grains. In some cases this is followed by euhedral quartz (5–20 μm).

Postdating quartz is a fine-grained calcite (4–100 μm; <1% of total rock composition) that hosts single-phase aqueous inclusions (Fig. 5), or aqueous-dominated inclusions with a miniscule bubble. The fine-grained calcite is postdated by up to 5 μm-thick chlorite cement. This is followed by clear coarse-grained calcite (up to 1000 μm) that engulfs fine sand grains and silt particles. The latter calcite is host to two-phase

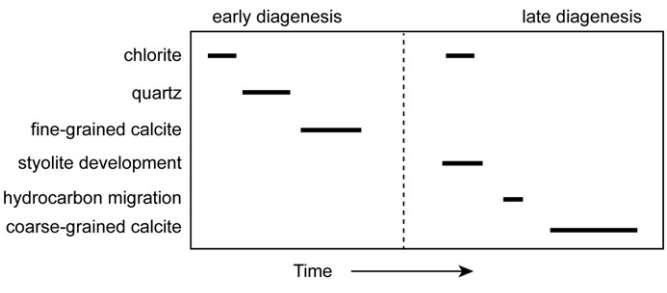

Fig. 4. Cement paragenesis showing timing of relative growth of early- and late-stage cements in addition to styolite development and hydrocarbon migration.

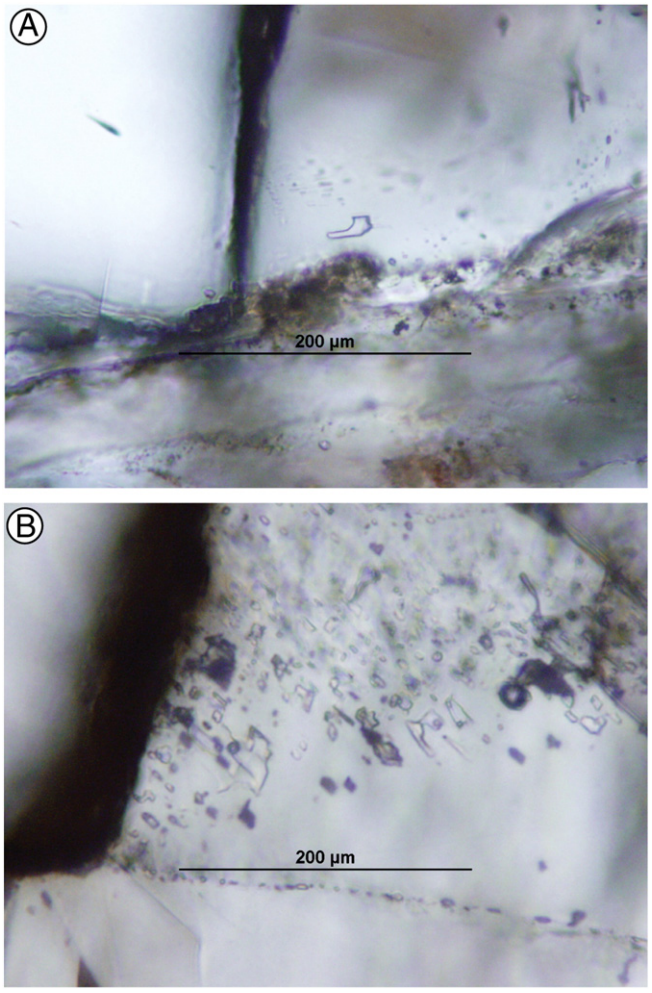

Fig. 5. Examples of primary fluid inclusions from (A) Stage 1 calcite where inclusions are generally one phase aqueous (implying near-surface trapping temperatures), and (B) Stage 2 where inclusions are two-phase aqueous dominated and T*h* values are in the 91.7 to 120.7 °C range. In (B) the fluid inclusion veil terminates at the surface of the wafer. The scale bar for both photomicrographs is 200 μm.

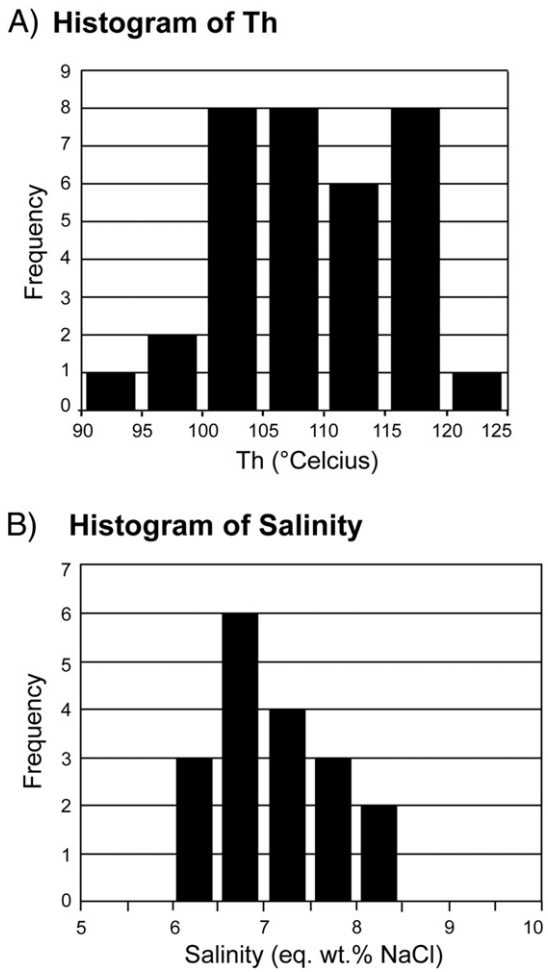

Fig. 6. Histograms of (A) homogenization temperatures from all primary fluid inclusions in the second calcite stage (n = 34) and (B) calculated estimates of salinity based on temperature measurements for the melting depression of ice (n = 18).

fluid inclusions with a visually estimated 97% aqueous phase and 3% vapor bubble by volume (Fig. 5). Some fluid inclusion trails are observed on either side of detrital grains confirming that the calcite engulfed the sediment's grains. Visual estimates of calcite can be as much as 10% in the coarse-grained sandstones or gritty horizons whereas the fine-grained sandstones lack pore space infilled by calcite.

Sparse ilmenite grains that are generally 100–200 μm in size all have a 5–20 μm coating of sphene (identified by MLA; Fig. 3C). Rather than growth of sphene, the sphene appears to form by pseudomorph replacement.

4.2. Fluid inclusion microthermometry of cements

The cements of the North Brook Formation consist of chlorite, quartz and calcite with the chlorite cements not hosting any visible inclusions. The early fine-grained calcite cement generation hosts single phase aqueous inclusions (Fig. 5), as well as aqueous-dominated (two-phase) fluid inclusions where the degree of fill is almost total that they are close to homogenization at room temperature. Performing ice-melting temperatures on such small monophase inclusions is almost impossible and freezing of such inclusions will stretch the inclusions, hence no salinity values are available for the early calcite.

The late-stage coarse calcite phase engulfs sand grains and host aqueous-dominated two-phase primary inclusions (Fig. 5). Primary fluid inclusion trails occur as straight zones, parallel to crystal facets, that terminate against detrital quartz grains and in back-scattered mode under the SEM, are associated with zones that are subtly darker than the remainder of the calcite crystals. Inclusions are sufficiently large to allow microthermometric examinations and measurements of homogenization temperatures (T*h*'s), ice-melting temperatures and calculations of estimates of salinity (Fig. 6). The T*h*'s range from 91.7 to 120.7 °C (109.0 ± 7.1 °C, $n = 34$). The calculated estimates of salinities range from 6.3 to 8.4 eq. wt.% NaCl (7.2 ± 0.4 eq. wt.% NaCl, $n = 18$), however, there is no correlation with T*h*. In a few cases, it was possible to document the transition of hydrohalite to brine plus ice in the −27.2 to −30.1 °C range. Assuming a NaCl–$CaCl_2$ system, this translates into a Ca:Na ratio of between 1:1 and 3.5:1 (Shepherd et al., 1985).

4.3. Fluid inclusion gas analysis of cements

The fluid inclusion gas analysis was performed by the cold crush fast scan. Since the samples are heterogeneous with multiple minerals, there is concern whether crushes liberate exclusively calcite-hosted inclusions or whether quartz-hosted inclusions contaminate the crushes. It is likely that initial incremental crushes of sandstone samples will liberate calcite cement hosted inclusions first owing to the soft nature of calcite. Progressive incremental crushing may possibly become contaminated by inclusions hosted in harder detrital minerals, mainly quartz. To assess this issue, quartz was separately analyzed. A partly crushed sandstone sample was subjected to 1 m HCl for 1 day to dissolve the calcite cement. The sample was washed with deionized water and after drying, the quartz grains were hand-picked using a binocular microscope. Approximately 25 mg of quartz was recovered that yielded 4 incremental bursts during crushing under vacuum (Tables 2 and 3). All 4 quartz inclusion analyses have high CO_2 and plot in separate fields from the regular crushes on all diagrams. As no inclusions were observed in other detrital mineral phases, we therefore assume that the fluid inclusion bursts represent the calcite inclusion gas chemistry.

Valuable information can be obtained from fluid inclusion gas chemistry relating to geothermal systems, including fluid sources (Norman and Moore, 1997; Blamey, 2012). Although recently applied to diagenetic carbonates (Azmy and Blamey, 2013), this current study reveals a broad CO_2/CH_4 range of 0.56 to 22 as well as a broad N_2/Ar ratio. It might be expected that fluid chemistry would remain constant but this is not the case with the North Brook diagenetic fluid inclusions (Tables 2 and 3 and Fig. 7). Individual sample analyses have some degree of overlap with other samples but fluid compositions are clearly heterogeneous and do not show contributions from the detrital quartz grains (Fig. 7).

Table 2
Quantitative fluid inclusion gas analyses of individual crushes for the quartz separate sample by the incremental crush method. Data is reported in mol percent for all species whereas the burst size for individual crushes represents the total current in amps generated by the mass spectrometer.

Crush#	H_2	He	CH_4	H_2O	N_2	O_2	Ar	CO_2	Burst
8686d	0.0032	0.0041	0.0641	94.898	0.3739	tr	0.0078	4.6498	8.69e-7
8686e	0.0062	0.0025	0.0508	94.0545	0.2103	tr	0.0038	5.6719	1.81e-7
8686f	0.0099	0.0020	0.0459	93.8823	0.3082	tr	0.0067	5.7450	2.49e-7
8686g	0.0164	0.0032	0.0648	94.3781	0.4689	tr	0.0109	5.0578	4.18e-7

Table 3
Quantitative fluid inclusion gas analyses of individual crushes for the sandstone samples by the incremental crush method. Data is reported in mol% for all species whereas the burst size for individual crushes represents the total current in amps generated by the mass spectrometer.

Sample#	H_2	He	CH_4	H_2O	N_2	O_2	Ar	CO_2	Burst
1-749a	0.0000	0.0024	0.0609	98.574	0.536	tr	0.0053	0.738	1.38e-8
1-749b	0.0000	0.0017	0.1032	96.3842	1.1748	tr	0.0135	2.27	6.67e-8
1-749c	0.0000	0.0052	0.2694	95.6705	1.4983	tr	0.0124	2.480	8.10e-8
1-749d	0.0000	0.0169	0.2833	95.4957	1.2607	tr	0.0131	2.885	2.50e-7
1-790a	0.0000	0.0003	0.1311	98.799	0.4525	tr	0.0023	0.5445	1.73e-8
1-790b	0.0000	0.0005	0.3402	99.0455	0.2446	tr	0.0053	0.190	7.10e-9
1-790c	0.0000	0.0003	0.0995	99.259	0.4064	tr	0.0048	0.133	7.93e-9
1-790d	0.0000	0.0046	0.305	96.992	1.3042	tr	0.0128	1.33	2.73e-7
1-790e	0.0000	0.0055	0.325	96.279	1.3735	tr	0.0133	1.952	3.09e-7
1-800a	0.0000	0.0002	0.0324	96.1803	1.1435	tr	0.0083	2.418	5.38e-8
1-800b	0.0000	0.0006	0.0519	95.4796	1.3423	tr	0.0104	2.976	6.33e-7
1-800c	0.0000	0.0012	0.0484	96.096	1.2075	tr	0.0075	2.544	8.55e-7
1-800d	0.0000	0.0008	0.0509	97.8461	0.8497	tr	0.0062	1.180	1.61e-6
1-855a	0.0000	0.0007	0.1723	98.637	0.4305	tr	0.0044	0.685	5.04e-8
1-855b	0.0000	0.0039	0.5258	96.6453	0.5223	tr	0.0086	2.27	3.25e-6
1-855c	0.0000	0.0047	0.6292	96.0434	0.5274	tr	0.0058	2.771	4.18e-6
1-855d	0.0000	0.0038	0.7402	93.2347	0.9345	tr	0.0136	5.049	3.23e-6
1-904a	0.0000	0.0007	0.0512	99.4418	0.079	tr	0.0009	0.4039	1.31e-8
1-904b	0.0000	0.0009	0.065	99.3039	0.0651	tr	0.0009	0.5478	1.19e-7
1-904c	0.0000	0.0010	0.0698	99.3578	0.0666	tr	0.0012	0.486	1.88e-7
1-904d	0.0000	0.0004	0.0473	99.4541	0.0308	tr	0.0008	0.451	7.87e-8
1-904e	0.0000	0.0007	0.0524	99.4273	0.0321	tr	0.0007	0.4726	2.73e-7
1-904f	0.0000	0.0008	0.0999	99.2753	0.0384	tr	0.0007	0.5586	1.55e-8
1-916a	0.0000	0.0018	0.0949	98.7822	0.5548	tr	0.0075	0.5196	5.39e-8
1-916b	0.0000	0.0012	0.1082	98.6805	0.7519	tr	0.0065	0.4109	8.92e-8
1-916c	0.0000	0.0005	0.0457	99.3223	0.2881	tr	0.0029	0.1866	1.37e-8
1-916d	0.0000	0.0005	0.0889	99.2997	0.3777	tr	0.0059	0.1606	8.84e-9

4.4. Cathodoluminescence

Examination of calcite cements by cathodoluminescence (CL) reveals concentric zonation (Samples 1-799, 1-855, and 1-964) exhibiting bright to orange CL by zones adjacent to authigenic grains and dull CL in the cores (Fig. 8). The lighter zones correlate with the early meteoric calcite cements whereas the darker cores correlate with the deep burial calcite cements.

4.5. Trace element and REE analysis by SIMS

Calcite cements in sample 1-800 were identified and analyzed by SIMS for Ca, Na, Mn, Fe, Sr, U, Th, and several rare earth elements (Table 4). The Mn content is noticeably enriched in Stage 1 calcite relative to Stage 2 by orders of magnitude (Fig. 9). The mean for Mn in Stage 1 is 8942 ppm (range is 3941 to 17,720 ppm) whereas the Stage 2 calcite range is 32 to 99 ppm and averages 63 ppm (Fig. 9).

The Stage 1 Sr varies from 96 to 218 ppm with a mean of 146 ppm whereas the Stage 2 Sr exhibits greater variation, ranging from 95 to 426 ppm with a mean of 319 ppm (Fig. 9). Fe ranges from 126 to

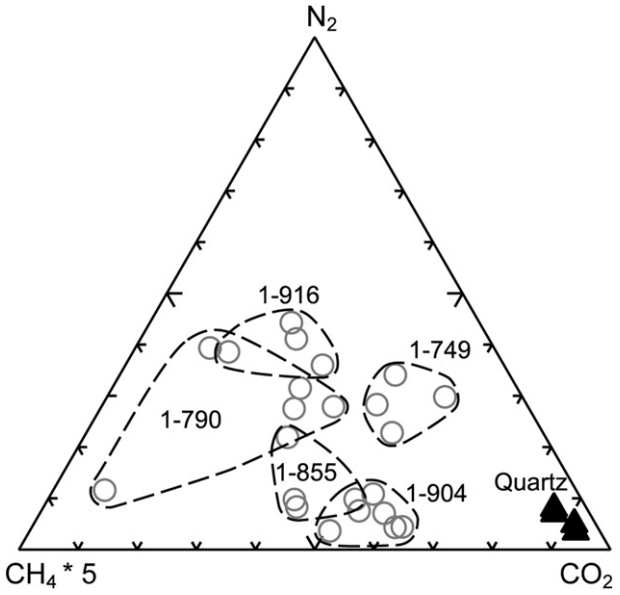

Fig. 7. Ternary CH_4–N_2–CO_2 plot of fluid inclusion gases. The dark triangle symbols that plot in the bottom right corner represent the quartz separate data whereas the gray circles correspond to the calcite cement analyses.

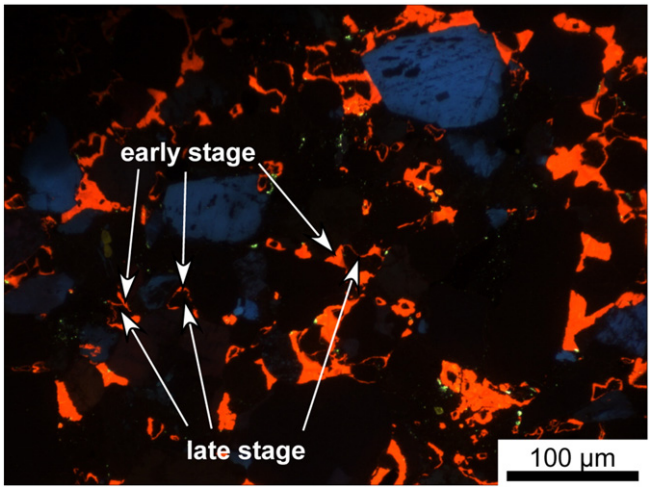

Fig. 8. Cathodoluminescence (CL) image showing zoned calcite (Sample 1-964). The bright CL (orange) corresponds to the early stage calcite, including the meteoric phase, whereas the dull cores correspond to the deep burial calcite.

Table 4
Trace element analyses of the calcite cements by secondary ion mass spectrometry. Mn/Fe ratios in the Stage 1 calcite cement are much higher than in the Stage 2 calcite cement.

Sample	Sr (ppm)	Mn (ppm)	Fe (ppm)	U (ppm)	Mn/Fe
Stage 1 Calcite					
1-800 ima5a	160	6645	126	1.14	53
1-800 ima5b	117	17,720	140	0.080	127
1-800 ima5e	139	10,885	130	1.11	84
1-800 Loc 4	218	3941	169	1.39	23
1-800 Loc 6	96	5518	147	1.57	38
Stage 2 Calcite					
1-800 ima5c	265	99	58	1.06	1.7
1-800 ima5d	95	81	64	1.03	1.3
1-800 Loc2	344	51	322	2.14	0.16
1-800 Loc3	397	59	71	1.14	0.83
1-800 Loc 5	389	55	113	1.28	0.49
1-800 Loc 7	426	32	53	1.17	0.60

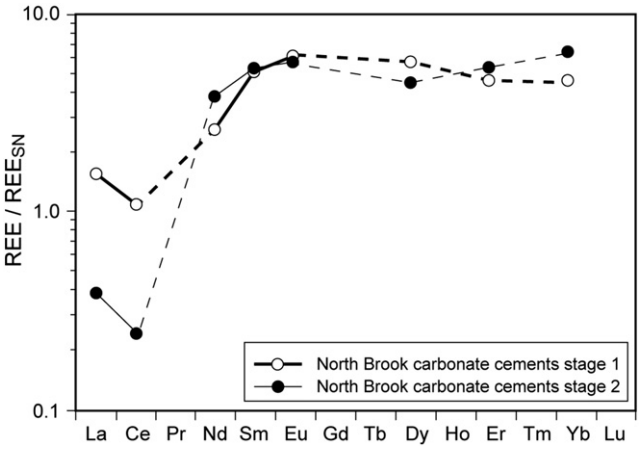

Fig. 10. Shale normalized (relative to PAAS) REE distribution patterns of stage 1 and 2 calcite cements from the North Brook Formation, Newfoundland. Both cements have similar patterns with slightly more depleted La and Ce in Stage 2 calcite.

169 ppm in stage 1 calcite whereas variability is greater in stage 2 calcite where the range is 53 to 322 ppm.

Rare Earth element analyses for the early and late stage calcite (Appendix 1 and Fig. 10). On the contrary, the concentration of most REEs in quartz is below the detection limit for SIMS. Both early and late calcite have very similar REE patterns with the distributions enriched relative to PAAS and slightly depleted in light REEs. A negative Cerium anomaly dominates the REE distribution and there is no significant Eu counterpart.

4.6. Stable isotope analysis

The C- and O-isotope measurements of the carbonate cements in North Brook formation are based on the signature of calcite cements of both stages (1 and 2) but the visual estimates of cement abundance indicates that the deep burial late coarse equant calcite (up to 10%) is much more dominant than the early diagenesis fine-grained early diagenesis counterpart (ca. ~1%). Therefore the $\delta^{13}C$ and $\delta^{18}O$ signature reflects mainly the composition of the late burial calcite cements. The $\delta^{13}C$ and $\delta^{18}O$ isotopes (Fig. 11) range generally from −6.0 to −3.5‰ VPDB (-4.75 ± 0.74, n = 17) and from −12.0 to −9.8‰ VPDB ($(-10.69 \pm 0.69$, n = 17) with distinct light values occurring at ~845 and ~904 m deep (Fig. 11).

5. Discussion

5.1. Cementation and diagenetic environments

The cements of different stratigraphic units exhibit the same paragenetic order whereby an assemblage of chlorite and calcite is repeated (Fig. 3). In the first cycle starts with a very thin chlorite coating,

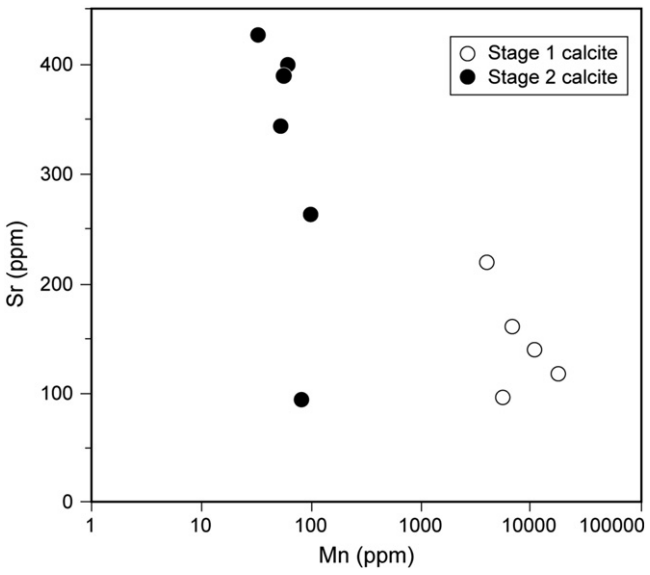

Fig. 9. Scatter diagram of Sr vs Mn for stage 1 & 2 calcite cements. All stage 1 Mn contents are greater than those of stage 2 by more than one order of magnitude. With the exception of two analyses, the Sr content is greater in Stage 2 cements than their stage 1 counterparts.

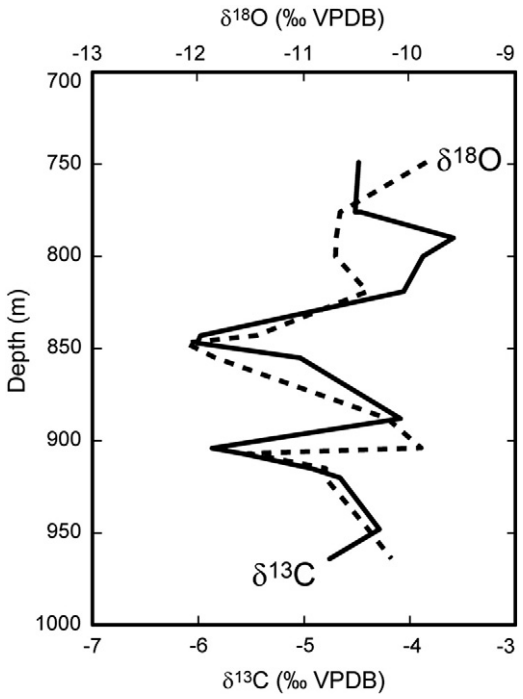

Fig. 11. $\delta^{13}C$ and $\delta^{18}O$ profiles of calcite cements showing parallel inflections particularly at ~845 and ~904 m depth. Detail in text.

which is consistent with the absence of quartz from the assemblage since chlorite retards the development of quartz cement (Peng et al., 2009). Quartz overgrowth (up to 20 μm euhedral crystals) occurs rarely at the exterior surface of detrital grains. It is clear that chlorite was effective in blocking nucleation and growth sites for quartz. The typical quartz cements occur within fractures that developed open space within feldspar grains. It is most likely that the feldspars cracked after the staining of chlorite, which exposed fresh surfaces for the nucleation of quartz.

Precipitation of quartz cement is normally associated with high-temperature (~192 °C) in relatively deep-burial diagenetic environments (e.g., Henley et al., 1984) although some recent studies (e.g. Walderhaug, 1994, 2000; Worden and Morad, 2009) documented precipitation at considerably lower temperatures (~100 °C). In geothermal systems, the theoretical solubility crossover between quartz and chalcedony occurs at 192 °C thus causing chalcedony to develop below 192 °C (Henley et al., 1984). In North Brook sandstones, quartz is associated with calcite that clearly formed at near-surface conditions, which would traditionally imply that chalcedony should have formed. However, quartz is known to precipitate at the expense of chalcedony under the presence of high organic content and it is not uncommon for quartz overgrowth or crystals to be associated with petroleum systems (Parnell et al., 1996). Limited quartz growth may have allowed petroleum migration and high fluid volumes during the first cementation cycle (Worden et al., 1998; Marchand et al., 2000, 2001, 2002).

The armoring of ilmenite by sphene suggests that the replacement process occurred in situ. If replacement occurred during transport or in the provenance area, then sphene would not have surrounded the ilmenite grains. In addition, to form sphene that replaces ilmenite, silica must have been added. The only other silica growth occurred when quartz precipitated during the first cementation cycle hence replacement of ilmenite by sphene was potentially coeval with quartz cementation owing to high silica activity.

The quartz overgrowth is followed by the precipitation of fine-grained calcite which hosts mono-phase aqueous primary fluid inclusions. The calcite crystals are clear and generally vary in size between 30 and 40 μm. This fine-grained calcite is not ubiquitous in the formation and in some samples calcite is absent.

The fine-grained calcite cement is followed by chlorite cement from the second cementation cycle and occurs as a stain or up to 20 μm-thick lamina where chlorite grows radially outwards from the surface of grains (Peng et al., 2009). To form chlorite requires unusual conditions where Fe is present thus enhancing the stability of chlorite instead of other clay minerals, as is the case in the Danish North Sea (Stokkendal et al., 2009). Although rare chlorite grains are observed in the sediment pile, they are considered insufficient to provide enough Fe for chlorite formation. However, accessory Fe-oxides in the form of martite (hematite) that replaces magnetite occurs, which may imply that the process of replacement may have provided a source of Fe that stabilized chlorite. Under strong oxidizing conditions martite is highly insoluble whereas under reducing conditions Fe may be taken into solution as ferrous ion (Fe^{2+}). It is likely that the redox conditions allowed enough Fe^{2+} to enter solution. The timing of the second generation of chlorite cement generation remains uncertain.

The final cementation event is the precipitation of coarse-grained (up to 1000 μm) calcite infilling. Twinning planes are seen to continue uninterrupted on either side of sediment grains, suggesting that calcite engulfs the sediment grains in-situ. Unlike the fine-grained calcite phase that contained all-liquid inclusions, the coarse-grained calcite hosts two-phase aqueous-dominated fluid inclusions with T*h* ranging between 91.7 and 120.7 °C which are typical of a deep burial origin (e.g., Azmy et al., 2009, 2011). The T*h*'s reflect the minimum temperature estimates of precipitation for those calcite cements. Similar to the calcite twinning that is continued across clasts and grains, primary fluid inclusion trails also continue on either side of sedimentary grains thus indicating that the sedimentary grains were engulfed by the coarse-grained calcite.

Two repeated events are inferred from the presented cement evidence, both starting with chlorite and ending with calcite. The first sequence developed a chlorite staining which may have been insufficient in places to block grain surfaces thus allowing occasional quartz overgrowths. Chlorite cements have been found in some earlier studies to inhibit the nucleation of quartz cements (Peng et al., 2009), thus maintaining the porosity during diagenesis. The monophase aqueous fluid inclusions in the early fine-grained calcite phase suggest precipitation under near surface conditions (T < 50 °C) likely in meteoric phreatic environment.

The second sequence has thicker chlorite which might have blocked all sites for quartz overgrowth, thus restricting quartz cements to the first cycle in the paragenetic sequence. Calcite infilling has occurred at elevated temperatures associated with warm brines of deeper burial settings. Fluid inclusion isochors calculated for the NaCl–H_2O system (Fig. 12) with minimum, maximum and average fluid inclusion T*h*'s in addition to minimum and maximum estimated geothermal gradients of 20 and 30 °C/km. A geothermal gradient of 25 °C/km is inferred by Azmy et al. (2009) based on the alteration index of conodonts and thus provides a realistic value for the area. The intersection of the average fluid inclusion T*h* and the 25 °C/km geothermal gradient corresponds to an approximate trapping P-T environment of 130 °C and 500 bar pressure. Temperatures were therefore on the upper limit for the oil window. Lithostatic conditions are unlikely in uncemented sediments and we assume hydrostatic conditions of 5 km depth.

Precipitation of calcite is controlled by several factors, including a reversed solubility that causes calcite to be less soluble with increasing temperature. Calcite precipitation can be understood by the following equilibrium reaction:

$$Ca^{2+} + 2HCO_3^- = CaCO_3 + H_2O + CO_2$$

Hydrohalite melting to ice indicates that for some inclusions, Ca^{2+} must have been high (Shepherd et al., 1985) and potentially induced calcite precipitation. However, calcite precipitation would have caused carbonic acid to form, thus making the fluid slightly more acidic. Further data is required to fully understand the mechanism of

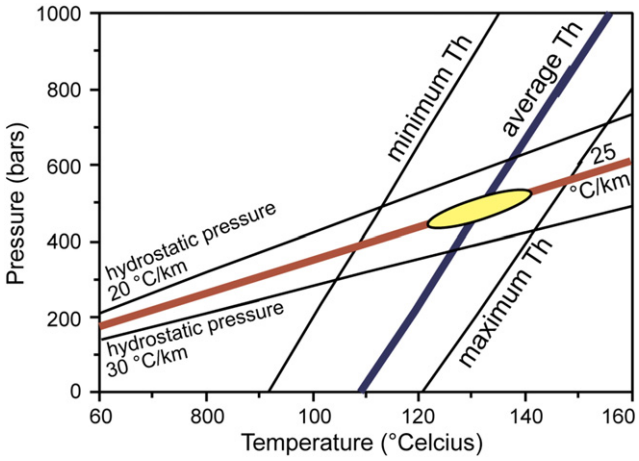

Fig. 12. Fluid inclusion pressure–temperature correction diagram showing isochors for the NaCl–water system based on the minimum, maximum and average homogenization temperatures. Also shown are the hydrostatic geothermal gradients and expected limits of 20 and 30 °C/km; a geothermal gradient of 25 °C/km is proposed by Azmy et al. (2009) based on the alteration index of conodonts. Details in text.

Appendix 1 Samples with Sr, Mn, Fe and REE composition from Northbrook.

McLennan 1989						Values normalized to the PAAS										
Sample #	Sr	Mn	Fe	La (ppb)	Ce	Pr	Nd	Sm	Eu	Gd	Tb	Dy	Ho	Er	Tm	Yb	Lu	Total REE (ppm)
North Brook diagenetic cements stage 2																		
1-800 Ima 5c CC REE Apr 5 2011	265	99	58	19573.6	33167.8		254219.6	62191.7	12368.0			48006.7		28517.9		37569.4		495.6
1-800 Ima 5d CC REE Apr 5 2011	95	81	64	48264.2	73922.5		335567.0	71219.6	14772.5			49774.5		24828.3		32001.0		650.3
1-800 Loc 2 CC REE April 5 2011	344	51	322	19573.6	4812.0		27901.8	2328.4	1171.2			0.0		0.0		956.7		56.7
1-800 Loc 3 CC REE April 5 2011	397	59	71	1610.7	1532.7		36853.2	7070.9	1999.3			11518.4		7231.5		4664.2		72.5
1-800 Loc 5 CC REE April 5 2011	389	55	113	281.6	2265.1		30422.8	8842.0	3037.4			5667.9		11913.7		0.0		62.4
1-800 Loc 7 CC REE April 5 2011	426	32	53	390.1	1027.0		86903.9	23593.4	3466.8			10851.3		19643.8		35002.9		180.9
North Brook diagenetic cements stage 1																		
1-800 Ima 5a CC REE Apr 5 2011	160	6645	126	58861.8	90197.7		121843.4	29018.9	5856.5			24141.2		9464.7		13206.8		352.6
1-800 Loc 6 CC REE April 5 2011	96	5518	147	22287.0	35804.1		29897.2	13622.4	3674.4			9056.9		7324.8		1154.4		122.8
1-800 Loc 4 CC REE April 5 2011	218	3941	169	101610.6	125231.7		140735.8	55051.6	11111.8			63764.1		29244.3		30701.9		557.5
1-800 Ima 5b CC REE Apr 5 2011	117	17,720	140	27365.1	42485.7		34282.3	11659.8	3407.2			11879.3		7253.6		9261.1		147.6
1-800 Ima 5e CC REE Apr 5 2011	139	10,885	130	92147.7	138080.2		116339.3	32319.2	8744.9			24151.3		11976.2		9937.7		433.7

		McLennan 1989						Values normalized to the PAAS										
		PAAS = Post-Archean Australian Shale (ppm)																
		38.200	79.600	8.830	33.900	5.550	1.080	4.660	0.774	4.680	0.991	2.850	0.405	2.820	0.433	ppm		
Th	U	La	Ce	Pr	Nd	Sm	Eu	Gd	Tb	Dy	Ho	Er	Tm	Yb	Lu	Total REE (ppm)	Ce/Ce*	Pr/Pr*
North Brook diagenetic cements stage 2																		
	1064.9	0.5124	0.4167	0.0000	7.4991	11.2057	11.4518	0.0000	0.0000	10.2578		10.0063	0.0000	13.3225			1.6264	3.7496
	1027.9	1.2635	0.9287	0.0000	9.8987	12.8324	13.6783	0.0000	0.0000	10.6356		8.7117	0.0000	11.3479			1.4701	4.9494
	2138.1	0.5124	0.0605	0.0000	0.8231	0.4195	1.0844	0.0000	0.0000	0.0000	0.0000	0.0000	0.0000	0.3392			0.2360	0.4115
	1135.5	0.0422	0.0193	0.0000	1.0871	1.2740	1.8512	0.0000	0.0000	2.4612		2.5374	0.0000	1.6540			0.9133	0.5436
	1279.1	0.0074	0.0285	0.0000	0.8974	1.5932	2.8124	0.0000		1.2111		4.1803		0.0000			7.7198	0.4487
	1170.2	0.0102	0.0129	0.0000	2.5635	4.2511	3.2100	0.0000		2.3187		6.8926		12.4124			2.5270	1.2818
North Brook diagenetic cements stage 1																		
	1136.8	1.5409	1.1331	0.0000	3.5942	5.2286	5.4227	0.0000	0.0000	5.1584	0.0000	3.3210	0.0000	4.6833	0.0000		1.4708	1.7971
	1570.7	0.5834	0.4498	0.0000	0.8819	2.4545	3.4022	0.0000		1.9352		2.5701		0.4094			1.5419	0.4410
	1393.7	2.6600	1.5733	0.0000	4.1515	9.9192	10.2887	0.0000	0.0000	13.6248	0.0000	10.2612		10.8872			1.1829	2.0757
	803.7	0.7164	0.5337	0.0000	1.0113	2.1009	3.1548	0.0000	0.0000	2.5383	0.0000	2.5451	0.0000	3.2841	0.0000		1.4901	0.5056
	1108.2	2.4122	1.7347	0.0000	3.4318	5.8233	8.0971	0.0000	0.0000	5.1605	0.0000	4.2022	0.0000	3.5240	0.0000		1.4382	1.7159

calcite precipitation. However, we suggest that increasing temperature and high calcium ion concentration most likely facilitated calcite deposition.

On the other hand, meteoric water running through exposed carbonate rocks was possibly loaded by Ca^{2+}, which facilitated the precipitation of calcite cements through the burial of sediments. The discharge and recharge of the diagenetic fluids with Ca^{2+} ions and availability of CO_3^{2-} ions possible through the oxidation of available organic matter likely played a role in the distribution of calcite cements and the occlusion of pores with calcite in some impervious horizons of the sequence compared with other porous counterparts.

The Fe and Mn contents in calcite are the major factor that controls the degree of luminescence under cold cathodoluminoscope (e.g., Machel, 1985). The chemical composition, particularly those of Mn and Fe, of the diagenetic fluids vary through the course of cement precipitation. Manganese has been found to be an activator of luminescence but Fe a quencher. Therefore, the lower the molar Fe/Mn values are, the brighter (bright red to orange) the luminescence is and vice versa (Machel et al., 1991). The calcite cement crystals show concentric zoning (dark cores and bright rims) under CL (Fig. 8) and cores of crystals exhibit dull to no CL, which is likely caused by enrichment of Fe (higher Fe/Mn molar ratios) due to precipitation under reducing conditions of deep burial settings. On the contrary, the outer zones are bright red to orange, which is caused by lower molar Fe/Mn contents due to precipitation at shallower burial settings (Fig. 8). The fine-grained calcite (Fig. 5), which contains all-liquid fluid inclusions, exhibit bright luminescence, which is consistent with near-surface Fe-poor and less reducing diagenetic settings of meteoric environment.

5.2. Trace elements and REE's

The distribution of trace elements in stages 1 and 2 is derived from an analysis of SIMS (Table 1). The Mn content is orders of magnitude higher in stage 1 relative to stage 2 (Fig. 9) and is likely to be controlled by fluid redox.

The REE PAAS-normalized distributions (McLennan, 1989) for the early and late-stage calcites have similar and almost coinciding profiles (Fig. 9). As the late-stage calcite mimics the early calcite, we consider the possibility that the late-stage calcite REE's may have been sourced from the early calcite by the process of dissolution and reprecipitation. Alternatively REE patterns might reflect fluid equilibrating with sedimentary package and therefore reflecting the REE's of the sediments. In addition, it is noted that the REE profiles are mainly flat but slightly LREE-depleted whereas the HREEs are slightly less than 10 relative to PAAS, a profile not dissimilar to mid-ocean ridge basalt (MORB) and contrasts with the profile of material derived from hot spots where LREE's are enriched. However, the prominent Ce negative anomaly suggests a redox condition that resulted in Ce being scavenged under oxidizing conditions prior to calcite deposition. Alternatively, the Ce anomaly could be due to removal by Fe-hydroxides and possibly enriched in chlorite or sphene. The cement Ce anomalies contrast with REE profiles reported by Azmy et al. (2011) for brachiopods in equilibrium with Paleozoic seawater, suggesting that the REE distributions in calcite cements of the Northbrook were not influenced by seawater but rather by basinal fluids.

Both $\delta^{13}C$ and $\delta^{18}O$ isotopes exhibit distinct lighter signatures at depths of ~845 and ~904 m (Fig. 11). These depths correlate with gritty horizons where the porosity and permeability is likely to have been greater and also correlate with the greatest degree of calcite cementation. It is likely that these coarse sandstones acted as aquifers and that the migrating brines or potential hydrocarbon-bearing fluids have influenced the isotopic composition.

Chlorite linings and cements at an early stage of the diagenetic history became keys to maintaining open pore space by prevented or restricting the nucleation and growth of quartz cement. Previous studies did not investigate the origin of cement. Our current investigation using petrography and fluid inclusions analyses allowed us to identify two diagenetic environments by identifying chlorite and two different phases of calcite cements, one at early shallow meteoric environment and the other at deep burial settings from hot fluids. Temperatures during the second cementation cycle approximated to the upper limit of the oil window at a pressure of 500 bars (5 km depth hydrostatic), implying that the North Brook Formation could potentially have been a petroleum source or pathway. However, infilling by calcite cement during the second cycle is generally well developed and limits the North Brook sandstones from being potential petroleum reservoirs, except where pore space may exist elsewhere in the basin.

6. Conclusion

Fluid-inclusion studies of cements from the North Brook Formation of western Newfoundland reveal significant clues about the diagenetic and burial history of the basin. Chlorite cements have restricted the nucleation of quartz cements which maintained porosity and permeability until temperatures matched the oil window. The North Brook Formation sandstones exhibit 2 cycles of cementation of chlorite followed by calcite. The first cycle occurred at near-surface temperatures and oxidizing conditions likely of a meteoric diagenetic environment, whereas the second cycle occurred under deeper burial conditions at temperatures within the range of oil window (around 130 °C) and pressure around 500 bar (5 km hydrostatic pressure). The later calcite cementation greatly reduced the porosity of the North Brook Formation.

Trace element analysis by SIMS confirms relatively low Fe/Mn ratios and lower Sr content in early calcite whereas the later calcite has high Fe/Mn and a greater Sr content, reflecting reducing conditions. The cathodoluminescence zoning in the late burial cements reflects changes in the chemistry with progressive burial. The similarity in the normalized REE patterns of early and late cements suggests that REEs in late calcite cements were derived from the early calcite cements. Fluid inclusion gases within the calcite cements confirm that the redox was variable and that it is possible to liberate inclusions within calcite cements without contamination from inclusions hosted within detrital quartz grains.

No previous studies have recognized multiple cements nor provide their origin in the North Brook Formation.

Acknowledgments

The authors wish to thank the editor and reviewers for their constructive reviews. A special thanks to Dr. Elliott Burden for providing valuable thoughts and feedback relating to the North Brook Formation, Dr. James Conliffe for maintaining the calibration of the CREAIT microthermometry facility on campus, and Mr. Michael Schaffer for supervising the MLA lab. Mr. Mike Lozon is thanked for improving upon the figures using his drafting skills. This project was supported by funding (to Karem Azmy) from the Petroleum Exploration Enhancement Program (PEEP).

References

Aase, N.E., Walderhaug, O., 2005. The effect of hydrocarbons on quartz cementation: diagenesis in the Upper Jurassic sandstones of the Miller Field, North Sea, revisited. Petroleum Geoscience 11, 215–223.

Aase, N.E., Bjørkum, P.A., Nadeau, P.H., 1996. The effect of grain-coating microquartz on preservation of reservoir porosity. American Association of Petroleum Geologists Bulletin 80, 1654–1673.

Awadallah, S., 1988. Description and interpretation of Unit 2 of the North Brook Formation, Dear Lake Basin in Well Western Adventure #1 (WA#1). Unpublished Report, Deer Lake Oil and Gas, pp. 19.

Azmy, K., Blamey, N.J.F., 2013. Origin of diagenetic fluids inferred from fluid inclusion gas ratios. Chemical Geology 347, 246–254.

Azmy, K., Knight, I., Lavoie, D., Chi, G., 2009. Origin of the Boat Harbour dolomites of St. George Group in western Newfoundland, Canada: implications for porosity controls. Bulletin of Canadian Petroleum Geology 57, 81–104.

Azmy, K., Brand, U., Sylvester, P., Gleeson, S.A., Logan, A., Bitner, M.A., 2011. Biogenic and abiogenic low-Mg calcite (bLMC and aLMC): evaluation of seawater-REE composition, water masses and carbonate diagenesis. Chemical Geology 280, 180–190.

Berger, A., Gier, S., Krois, P., 2009. Porosity-preserving chlorite cements in shallow-marine volcaniclastic sandstones: evidence from Cretaceous sandstones of the Sawan gas field, Pakistan. American Association of Petroleum Geologists Bulletin 93, 595–615.

Billault, V., Beaufort, D., Baronnet, A., Lacharpagne, J.-C., 2003. A nanopetrographic and textural study of grain-coating chlorites in sandstone reservoirs. Clay Minerals 38, 315–328.

Blamey, N.J.F., 2012. Composition and evolution of crustal, geothermal and hydrothermal fluids interpreted using quantitative fluid inclusion gas analysis. Journal of Geochemical Exploration 116–117, 17–27.

Blamey, N.J.F., Parnell, J., Longerich, H.P., 2012. Understanding detection limits in fluid inclusion analysis using an incremental crush fast scan method for planetary science. Lunar and Planetary Science Conference, #1035.

Burden, E., Gillis, E., French, E., 2005. Tectonostratigraphy of an exhumed Blow Me Down Brook Formation hydrocarbon reservoir, Sluice Brook, western Newfoundland. Current Research (2005) Newfoundland and Labrador Department Natural Resources, Geological Survey, Report 05-1, pp. 63–71.

Cooper, M., Weissenberger, J., Knight, I., Hostad, D., Gillespie, D., Williams, H., Burden, E., Porter-Chaudhry, J., Rae, D., Clark, E., 2001. Basin evolution in Western Newfoundland: new insights from hydrocarbon exploration. American Association of Petroleum Geologists Bulletin 85, 393–418.

Denniston, R.F., Shearer, C.K., Layne, G.D., Vaniman, D.T, 1997. SIMS analyses of minor and trace element distributions in fracture calcite from Yucca Mountain, Nevada, USA. Geochimica et Cosmochimica Acta 61, 1803–1818.

Friis, H., Sylvestersen, R.L., Nebel, L.N., Poulsen, N.L.K., Svendsen, J.B., 2010. Hydrothermally influenced cementation of sandstone — An example from deeply buried Cambrian sandstones from Bornholm, Denmark. Sedimentary Geology 227, 11–19.

Friis, H., Molenaar, N., Varming, T., 2013. Chlorite meniscus cement — implications for diagenetic mineral growth after oil emplacement. Terra Nova. http://dx.doi.org/10.1111/ter.12061 (in press).

Henley, R.W., Truesdell, A.H., Barton Jr., P.B., 1984. Fluid-equilibria in hydrothermal systems. Reviews in Economic Geology 2, 267.

Hyde, R.S., 1983. Geology of the Carboniferous Deer Lake Basin. Newfoundland Department of Mines and Energy, Mineral Development Division, Map 82-7. Scale 1:100000.

Hyde, R.S., 1984. Geological history of the Carboniferous Deer Lake Basin, west-central Newfoundland, Canada. In: Geltzer, H.H.J., Nassichuk, W.W., Belt, E.S., Mcqueen, R.W. (Eds.), Atlantic Coast basins, paleogeography and paleotectonics, sedimentology and geochemistry. Ninth International Congress of Carboniferous Stratigraphy and Geology. Carbondale, Illinois, vol. 3, pp. 85–104.

Hyde, R.S., 1989. The North Brook Formation: A temporal bridge spanning contrasting tectonic regimes in the Deer Lake Basin, Western Newfoundland. Atlantic Geology 25, 15–22.

Hyde, R.S., Miller, H.G., Hiscott, R.N., Wright, J.A., 1988. Basin architecture and thermal maturation in the strike-slip Deer Lake Basin, Carboniferous of Newfoundland. Basin Research 1, 85–105.

Irving, E., Strong, D.F., 1989. Paleomagnetism of the Early Carboniferous Deer Lake Group, western Newfoundland: no evidence for mid-Carboniferous displacement of "Acadia". Earth and Planetary Science Letters 69, 379–390.

Karim, A., Pe-Piper, G., Piper, D.J.W., 2010. Controls on diagenesis of Lower Cretaceous reservoir sandstones in the western Sable Subbasin, offshore Nova Scotia. Sedimentary Geology 224, 65–83.

Kim, J.C., Lee, Y.I., Hisada, K.-I., 2007. Depositional and compositional controls on sandstone diagenesis, the Tetori Group (Middle Jurassic–Early Cretaceous), central Japan. Sedimentary Geology 195, 183–202.

Knight, I., 1983. Geology of the Carboniferous Bay St. George Subbasin, Western Newfoundland. Mineral Development Division. Department of Mines and Energy, Government of Newfoundland and Labrador, p. 358.

Knight, I., 2003. Geology of the North Brook anticline, Harry's River map area (NTS 12B/09). Current Research (2003) Newfoundland Department Mines and Energy, Geological Survey, Report 03-1, pp. 51–71.

Knight, I., Boyce, W.D., 2002. Lower Paleozoic carbonate rocks of the northern closure of the North Brook anticline and the Spruce Pond Klippe, Georges Lake (12B/16) and Harrys River (12B/9) map areas: collected thoughts on unconnected rocks. Current Research (2002) Newfoundland Department of Mines and Energy, Geological Survey, Report 02-1, pp. 121–134.

Langdon, G.S., Hall, J., 1994. Devonian–Carboniferous tectonics and basin deformation in the Cabot Strait area, Eastern Canada. American Association of Petroleum Geologists Bulletin 78, 1748–1774.

Larsen, O.H., Friss, H., 1991. Petrography, diagenesis and pore-water evolution of a shallow marine sandstone (Hasle Formation, Lower Jurassic, Bornholm, Denmark). Sedimentary Geology 72, 269–284.

Machel, H.G., 1985. Cathodoluminescence in calcite and dolomite and its chemical interpretation. Geoscience Canada 12, 139–147.

Machel, H.G., Mason, R.A., Mariano, A.N., Mucci, A., 1991. Causes and emission of luminescence in calcite and dolomite. In: Barker, C.E., Kopp, O.C. (Eds.), Luminescence microscopy: quantitative and qualitative aspects. Society of Economic Paleontologists and Mineralogists, Short Course notes, 25, pp. 9–25.

Mansurbeg, H., Morad, S., Salem, A., Marfil, R., El-ghali, M.A.K., Nystuen, J.P., Caja, M.A., Amorosi, A., Garcia, D., La Iglesia, A., 2008. Diagenesis and reservoir quality evolution of Palaeocene deep-water, marine sandstones, the Shetland–Faroes Basin, British continental shelf. Marine and Petroleum Geology 25, 514–543.

Marchand, A.M.E., Haszeldine, R.S., Macaulay, C.I., Swennen, R., Fallick, A.E., 2000. Quartz cementation inhibited by crestal oil charge: Miller deep water sandstone, UK North Sea. Clay Minerals 35, 205–214.

Marchand, A.M.E., Haszeldine, R.S., Smalley, P.C., Macaulay, C.I., Fallick, A.E., 2001. Evidence for reduced quartz cementation rates in oil-filled sandstones. Geology 29, 915–918.

Marchand, A.M.E., Smalley, P.C., Haszeldine, R.S., Fallick, A.E., 2002. Note on the importance of hydrocarbon fill for reservoir quality prediction in sandstones. American Association of Petroleum Geologists Bulletin 86, 1561–1571.

McBride, E.F., 1989. Quartz cement in sandstones: a review. Earth-Science Reviews 26, 69–112.

McLennan, S.M., 1989. Rare earth elements in sedimentary rocks: influence of provenance and sedimentary processes. In: Lipin, B.R., McKay, G.A. (Eds.), Geochemistry and Mineralogy of Rare Earth Elements. Reviews in Mineralogy, 21, pp. 169–200.

Norman, D.I., Blamey, N.J.F., 2001. Quantitative gas analysis of fluid inclusion volatiles by a two mass spectrometer system: European current research on fluid inclusions, no. XVI, Porto, Portugal. Abstracts 341–344.

Norman, D.I., Moore, J.N., 1997. Gaseous species in fluid inclusions: a fluid tracer and indicator of fluid processes: European current research on fluid inclusions, no. XIV, Nancy, France. Abstracts 243–244.

Parnell, J., Carey, P.F., Monson, B., 1996. Fluid inclusion constraints on temperatures of petroleum migration from authigenic quartz in bitumen veins. Chemical Geology 129, 217–226.

Parry, W.T., Blamey, N.J.F., 2010. Fault fluid composition from fluid inclusion measurements, Laramide age Uinta thrust fault, Utah. Chemical Geology 278, 105–119.

Peng, J., Liu, J., Wang, Y., Liu, J., 2009. Origin and controlling factors of chlorite coatings — an example from the reservoir of T3x Group of the Baojie area, Sichuan Basin, China. Petroleum Science 6, 376–382.

Ramm, M., Forsberg, A.W., 1991. Porosity vs. depth trends in Upper Jurassic sandstones from the Cod Terrace area, central North Sea. In: Ramm, M. (Ed.), Porosity Depth Trends in Reservoir Sandstones. University of Oslo, Norway (PhD thesis).

Shepherd, T.S., Rankin, A.H., Alderton, D.H.M., 1985. A practical guide to Fluid Inclusion Studies. Blackie & Son Ltd., Glasgow, p. 239.

Stokkendal, J., Friis, H., Svendsen, J.B., Poulsen, M.L.K., Hamberg, L., 2009. Predictive permeability variations in a Hermod sand reservoir, Stine Segments, Siri Field, Danish North Sea. Marine and Petroleum Geology 26, 397–415.

Tang, Z., Parnell, J., Longstaffe, F.J., 1997. Diagenesis and reservoir potential of Permian–Triassic fluvial/lacustrine sandstones in the southern Junggar Basin, northwestern China. American Association of Petroleum Geologists Bulletin 81, 1843–1865.

Vagle, G.B., Hurst, A., Dypvik, H., 1994. Origin of quartz cements in some sandstones from the Jurassic of the Inner Moray Firth (UK). Sedimentology 41, 363–377.

Walderhaug, O., 1994. Precipitation rates for quartz cements in sandstones determined by fluid-inclusion microthermometry and temperature-history modeling. Journal of Sedimentary Research A64, 324–333.

Walderhaug, O., 2000. Modeling quartz cementation and porosity in Middle Jurassic Brent Group sandstones of the Kvitebjørn Field, northern North Sea. American Association of Petroleum Geologists Bulletin 84, 1325–1339.

Wang, Q., Zhuo, X., Chen, G., Li, X., 2008. Carbon and oxygen isotopic composition of carbonate cements of different phases in terrigenous siliciclastic reservoirs and significance for their origin: a case study from sandstones of the Triassic Yanchang Formation, southwestern Ordos Basin, China. Chinese Journal of Geochemistry 27, 249–256.

Weibel, R., Friis, H., Kazerouni, A.M., Svendsen, J.B., Stokkendal, J., Puolsen, M.L., 2010. Development of early diagenetic silica and quartz morphologies — Examples from the Siri Canyon, Danish North Sea. Sedimentary Geology 228, 151–170.

Williams, S.H., Burden, E.T., 1992. Thermal maturity of potential Paleozoic source rocks in western Newfoundland. Centre for Earth Resources Research Memorial University of Newfoundland, Report EL# 92-103-01-EG, p. 34.

Wolela, A.M., Gierlowski-Kordesch, E.H., 2007. Diagenetic history of fluvial and lacustrine sandstones of the Hartford Basin (Triassic–Jurassic), Newark Supergroup, USA. Sedimentary Geology 197, 99–126.

Worden, R.H., Oxtoby, N.H., Smalley, P.C., 1998. Can oil emplacement prevent quartz cementation in sandstones? Petroleum Geoscience 4, 129–137.

Worden, R.H., Morad, S., 2009. Quartz cementation in oil field sandstones: a review of the key controversies. In: Worden, R.H., Morad, S. (Eds.), Quartz Cementation in Sandstones. Blackwell Publishing Ltd, Oxford, UK.